INTERFACE

royalsocietypublishing.org/journal/rsif

Research

Cite this article: Stylianou A, Gkretsi V, Louca M, Zacharia LC, Stylianopoulos T. 2019 Collagen content and extracellular matrix cause cytoskeletal remodelling in pancreatic fibroblasts. *J. R. Soc. Interface* **16**: 20190226. http://dx.doi.org/10.1098/rsif.2019.0226

Received: 28 March 2019
Accepted: 24 April 2019

Subject Category:
Life Sciences–Engineering interface

Subject Areas:
bioengineering, biomaterials, biomechanics

Keywords:
atomic force microscopy, tumour desmoplasia, biomechanics, collagen, cancer-associated fibroblasts

Author for correspondence:
Triantafyllos Stylianopoulos
e-mail: tstylian@ucy.ac.cy

†Present address: Biomedical Sciences Program, Department of Life Science, School of Sciences, European University of Cyprus, 6, Diogenis Str, 2404 Engomi, Nicosia, Cyprus.

Electronic supplementary material is available online at https://dx.doi.org/10.6084/m9.figshare.c.4498937.

THE ROYAL SOCIETY PUBLISHING

Collagen content and extracellular matrix cause cytoskeletal remodelling in pancreatic fibroblasts

Andreas Stylianou[1], Vasiliki Gkretsi[1,†], Maria Louca[1], Lefteris C. Zacharia[2] and Triantafyllos Stylianopoulos[1]

[1]Cancer Biophysics Laboratory, Department of Mechanical and Manufacturing Engineering, University of Cyprus, Nicosia 1678, Cyprus
[2]Department of Life and Health Sciences, School of Sciences and Engineering, University of Nicosia, 1700 Nicosia, Cyprus

AS, 0000-0002-1641-1854

In many solid tumours a desmoplastic reaction takes place, which results in tumour tissue stiffening due to the extensive production of extracellular matrix (ECM) proteins, such as collagen, by stromal cells, mainly fibroblasts (FBs) and cancer-associated fibroblasts (CAFs). In this study, we investigated the effect of collagen stiffness on pancreatic FBs and CAFs, particularly on specific cytoskeleton properties and gene expression involved in tumour invasion. We found that cells become stiffer when they are cultured on stiff substrates and express higher levels of alpha-smooth muscle actin (α-SMA). Also, it was confirmed that on stiff substrates, CAFs are softer than FBs, while on soft substrates they have comparable Young's moduli. Furthermore, the number of spread FBs and CAFs was higher in stiffer substrates, which was also confirmed by Ras-related C3 botulinum toxin substrate 1 (*RAC1) mRNA* expression, which mediates cell spreading. Although stress fibres in FBs become more oriented on stiff substrates, CAFs have oriented stress fibres regardless of substrate stiffness. Subsequently, we demonstrated that cells' invasion has a differential response to stiffness, which was associated with regulation of Ras homologue family member (*RhoA)* and Rho-associated, coiled-coil containing protein kinase 1 (*ROCK-1*) mRNA expression. Overall, our results demonstrate that collagen stiffness modulates FBs and CAFs cytoskeleton remodelling and alters their invasion properties.

1. Introduction

In many malignant tumours, including tumours of the pancreas, colon and breast, a desmoplastic reaction is known to take place during progression [1,2]. Tumour desmoplasia is a cancer-specific type of fibrosis characterized by extensive production of extracellular matrix (ECM) proteins, such as collagen type I by tumour stromal cells, mainly fibroblasts (FBs) and cancer-associated fibroblasts (CAFs) [1]. As a result, desmoplasia stiffens the tumour tissue and thus, increases the compressive mechanical forces in the tumour's interior [3–5]. Although it has long been known that this fibrotic response inhibits drug delivery and enhances tumour progression and metastasis, the exact underlying mechanisms are still unclear [6,7].

ECM stiffening and transforming growth factor-β (TGF-β) activation contribute to the conversion of FBs to activated, contractile myofibroblasts, also known as CAFs in the case of the tumour microenvironment [8]. CAFs further stimulate synthesis of ECM proteins reinforcing desmoplasia and tumour stiffening [8,9]. Matrix stiffening, in turn, causes an increase in TGF-β activation [8,10], which further promotes FB conversion [11] suggesting a positive feedback loop. Apart from CAFs, interactions of FBs with cancer cells and the ECM also play a crucial role in tumour progression [12]. Nevertheless,

the effect of ECM stiffening has not, so far, been investigated in relation to morphodynamic, cytoskeletal or biophysical alterations of pancreatic stromal cells, which ultimately affect fundamental cellular processes related to cancer cell metastasis such as cell motility, adhesion and invasion into surrounding matrix [13,14].

In the present work, two (2D) and three (3D) dimensional collagen ECM models with varying collagen concentrations and thus, tunable stiffness were developed. In addition, atomic force microscopy (AFM), image processing techniques, *in vitro* cellular assays, including spreading and invasion assays, and molecular approaches, such as real-time polymerase chain reaction (PCR), were employed in order to investigate the effect of collagen stiffness on pancreatic FBs and CAFs. Finally, we study the effect of stiffness in the presence of TGF-β. Defining the mechanistic interactions between ECM stiffness and FBs/CAFs, can provide the basis for the development of novel treatments that target stromal components to reduce desmoplasia and improve drug delivery and efficacy [9,15–17].

2. Material and methods

2.1. Cell culture

Commercially available pancreatic native human FBs and CAFs (cat. nos. SC00A5 and CAF08, respectively, Neuromics) were cultured in MSC-GRO (VitroPlus III, low serum, complete, cat. no. SC00B1, Neuromics) medium in a 5% CO_2-incubator at 37°C.

2.2. Fixation and permeabilization

Cells were first fixed with 4% paraformaldehyde (PFA, cat. no. P6148, Sigma) for 20 min and then a permeabilization buffer containing phosphate-buffered saline (PBS, cat. no. LM-S2041, biosera), 2 mg ml^{-1} bovine serum albumin (cat. no. A2153, Sigma), and 0.1% Triton X-100 (cat. no. 9002-93-1, Sigma) was used for permeabilizing the cell membranes.

2.3. Cell immunostaining

The α-smooth muscle actin (α-SMA) expression of cells was assessed by staining with anti-α-SMA antibody (cat. no. ab5694, Abcam) and Alexa 647 anti-rabbit antibody (cat. no. ab150079, Abcam) as the secondary antibody. Briefly, cells were fixed with 4% PFA, washed with permeabilization buffer and incubated overnight at 4°C with anti-α-SMA antibody. Samples were then washed three times with the permeabilization buffer and incubated with Alexa 647 anti-rabbit secondary antibody for 1 h at room temperature. Finally, cells were washed again three times with the permeabilization buffer and incubated for 2 min with 4′,6-diamidino-2-phenylindole (DAPI, cat. no. 10236276001 ROCHE, Sigma).

For staining actin stress fibres, the above protocol was followed with a minor change. Cells were incubated with phalloidin (cat. no. 00027, Biotium) for 1 h at room temperature and no secondary antibody was added.

All coverslips were then mounted on a slide and observed under an Olympus BX53 fluorescent microscope equipped with an Olympus XM10 Monochrome CCD camera (1.4 megapixels) and UPLanFLN microscope objective lenses (40×/0.75 and 100×/1.30 oil). Also, appropriate Chroma Technology filters were employed for imaging DAPI, α-SMA and phalloidin, namely the 49000 ET-DAPI (ex. 359 nm, em. 481 nm), the 49006 ET-Cy5 (excitation: 649 nm, emission: 679 nm) and the 49004 ET-Cy3 (ex. 552 nm, em. 579 nm), respectively.

2.4. Stress fibres

The freeware tool *FilamentSensor* [18] was used to characterize the actin stress fibres from fluorescent images of phalloidin-stained cells. The F-actin filament structure of FBs and CAFs cultured on collagen substrates with different stiffness was reconstructed (different fibre orientations were represented with different colours) using the *FilamentSensor* tool. Stress fibre orientation was assessed using the order parameter $S = \cos 2\theta$ [19], where θ is the angle formed between each stress fibre of the cell with the long axis of the fitted ellipse. An isotropic cytoskeleton should have $S = 0$ and a fully aligned (along the major axis of the cell) cytoskeleton should have 1. Therefore, the higher the value of S, the more oriented the fibres become.

2.5. Spreading

FBs and CAFs were cultured on 24-well plates and incubated at 37°C for 30 and 40 min, respectively. The time point chosen for each cell line was the one at which approximately 50% of cells had spread [20]. For assessing cell morphology, cells were fixed in 4% PFA (cat. no. P6148, Sigma) and imaged with an Eclipse TS100 inverted microscope equipped with a digital camera (Olympus XC50 Color CCD camera, 5 megapixel) and a Nikon Ph1 DL 10× 0.25 phase microscope objective lens. We used the optical microscope images from the spread cells so as to measure the cells' circularity and in order to obtain quantified results from the cell spreading assay. The circularity is defined as circularity $= 4\pi((\text{area})/(\text{perimeter})^2)$ and it was measured using ImageJ (NIH). ImageJ calculates the circularity in the range of 0–1, where 1 is completely circular and 0 is highly polarized. The cells were divided into three subclasses: rounded (circularity = 0.66–1.0), half rounded (0.33–0.66) and completely spread (0–0.33). For quantifying the percentage of spread cells, at least 300 cells from five randomly selected fields were assessed. Three independent experiments were performed and results represent mean values from all three experiments.

2.6. Collagen I substrates (two-dimensional collagen substrates)

Type I collagen solution from rat tail (cat. no. C3867, Sigma) was mixed with 10% 10× minimal essential medium (MEM, cat. no. 21430020, Gibco) and distilled water so as to get a final collagen concentration of 0.5, 1.0 and 3.0 mg ml^{-1}. The pH was adjusted to 7.4 by adding 1N NaOH. Then, 13 mm glass coverslips (cat. no. L46R13, Agar Scientific) or 35 mm Petri dishes (Thermo Scientific) were coated with 200 µl of the collagen solution and incubated at 37C° for at least 30 min.

2.7. Three-dimensional collagen I gels

In order to form 3D collagen I gels of desired concentration and consequently of different stiffness we used a modification of previously published protocols [21,22]. Briefly, we added the desired amount of a high concentration collagen I solution (cat. no. 354249, Corning) so as to get a final collagen concentration of 0.5, 1.0 or 3.0 mg ml^{-1}, in a solution containing 10% 10× MEM (cat. no. 21430-020, Gibco), 1% human insulin solution (cat. no. I9278, Sigma), and distilled water. Then the pH was adjusted to 7.4 by adding 1N NaOH and the gels were allowed to solidify.

2.8. Atomic force microscopy

2.8.1. Collagen gels imaging

For imaging collagen I gels with AFM, 90 µl of the collagen solution (of the desired concentration), was flushed on 13 mm circular glass cover glasses (cat. no. AGL46R13, Agar Scientific). The samples were then incubated in a cell culture incubator for 30 min. Afterwards the samples were mounted on 15 mm

specimen AFM metal discs (cat. no. AGF7003, Agar Scientific) with double-sided adhesive tape and then they were left in room temperature for air drying. For high resolution imaging of collagen gels, AFM images of the samples were obtained in air using a Cypher ES^{TM} Environmental AFM microscope (Asylum Research) in intermittent (also named tapping) mode with AC160TS AFM probes (Olympus). The images were analysed using the ARgyle Light (Asylum Research, ver. 20113.1.4.9) and the WSxM 5.0 dev.2.1 [23] software. All images were acquired at a fixed resolution (512 × 512 data points) with scan rate between 0.5 and 1 Hz.

2.8.2. Mechanical properties characterization of live cells

Cells were cultured in 35 mm Petri dishes coated with collagen of different concentrations for 2 days in their culture medium. Before the AFM experiments, cells were washed twice with PBS, new complete culturing media was added, and were incubated in a cell culture incubator for 30 min. Petri dishes were then directly mounted on AFM sample plates. Young's modulus of cells was acquired by using the PicoPlus AFM system with silicon nitride probes with a round, ball-shape tip (CP-PNPL-BSG-A-5, sQube, 0.08 N m^{-1} spring constant). The cells Young's modulus was assessed by acquiring 8 × 8 points of force curves in an area of 5 × 5 µm near the centre of the cells (electronic supplementary material, figure S1) and by using the Hertz model (Poisson ratio equal to 0.5) and the freeware software AtomicJ. For the AFM nanoindentation technique a set point of 1 nN normal force at a 2 µm s^{-1} rate on each of the studied cells was used, while the maximum indentation depth was set to 600 nm. The experiments were performed in less than 40 min per experiment and at least 30 live cells per condition from three independent experiments were studied. Finally, attention was paid so that FBs and CAFs in all experimental conditions were handled in the same way, using the same AFM tips, indenting force, culture media and culture density.

2.8.3. Mechanical properties characterization of collagen substrates and collagen gels

For AFM mechanical properties characterization of the collagen I gels and substrates the PicoPlus AFM system with V-shaped silicon nitride probes (PNP-TR, Nanoword, 0.32 N m^{-1} spring constant) was used. All AFM experiments were obtained at room temperature under liquid (PBS) conditions. In an area of 5 × 5 µm, 8 × 8 points of force curves were collected and analysed by AtomicJ [24] so as to calculate the sample's Young's modulus using the Hertz model. The spring constant of all tips that were used in the study was assessed with the thermal tune method.

2.9. Assessment of collagen fibres diameters

For assessing collagen fibre diameter, AFM images were analysed using the WSXM software. A 8 × 8 grid was overlaid onto the collected images and fibre diameter was measured for all fibres within the grid-cells [25]. Collagen fibres that were extended in neighbouring grid-cells were measured only once. For each collagen sample, the histogram of fibre diameters was compiled to display the frequency of occurrence of each fibre diameter.

2.10. Cell spheroid formation

For the formation of FB and CAF spheroids the 'hanging drop' technique was used as described previously [21,22]. Briefly, after a 2 day incubation period in Petri dishes with pure medium or medium containing TGF-β (5 µg ml^{-1}), FBs and CAFs were collected by trypsinization and put in suspension at a concentration of 2.5 × 10^4 cells ml^{-1}. Hanging drops containing 500 cells each were formed on the inside of the cover of a culture dish.

2.11. Invasion assay

Formed spheroids were transferred with a glass Pasteur pipette into wells of a 96-well plate containing 0.5, 1.0, and 3.0 mg ml^{-1} collagen I gel. A Nikon Eclipse optical microscope, equipped with a CCD camera, was used to image the spheroids at time zero (immediately after spheroid transfer) and after 6 h incubation at 37°C. ImageJ software was used to assess spheroids' size (average of the major and minor axis length) at time 0 and 6 h so as to determine cell invasion through surrounding collagen [21] (electronic supplementary material, figure S2).

2.12. Cells culturing in three-dimensional collagen I gels

Cell suspension of 2.5 × 10^5 cells ml^{-1} in pure medium or TGF-β-containing medium (5 µg ml^{-1}) were added in collagen gels with different concentrations before being solidified [22]. Cells were cultured at 37°C for 2 days and were then treated with 1 mg ml^{-1} collagenase D (cat. no. 11088858001, Sigma-Aldrich) for 30 min at 37°C so as to remove collagen and collect cells. Cell suspensions were then centrifuged at 300*g* for 5 min to remove digested collagen and cell pellets were kept for gene expression analysis.

2.13. RNA isolation and real-time polymerase chain reaction

Trizol (cat. no. 15596026, ThermoFisher Scientific) was used for extracting total RNA from the cells, which was subsequently, purified using RNeasy mini kit (cat. no. 74104, Qiagen) and transcribed to cDNA using Superscript III Reverse Transcriptase (cat. no. 18080093, Thermo-Fisher Scientific). Real-time PCR (CFX96 Real-Time PCR, BioRad) was used for the quantification of gene expression. The ΔΔCt method was used for quantifying the relative gene expression and all the reactions were done in triplicate for at least three independent experiments. All primers used are shown in electronic supplementary material, table S1.

2.14. Statistical analysis

Comparison of means with standard errors was used for the statistical analysis, while Student's *t*-test with $p < 0.05$ was regarded as statistically significant and each experimental group was repeated at least three times. Also, the 'multiple sample comparison' test was performed using Statgraphics 5.0 (software). After a significant difference was detected between the groups as evidenced from the ANOVA table a 'multiple range test' was performed to indicate the differences between groups.

3. Results

3.1. Matrix stiffening increases Young's modulus of fibroblasts and cancer-associated fibroblasts

We first set out to characterize the two human pancreatic cell lines, FBs and CAFs, in terms of cell morphology. Optical microscopy imaging demonstrated that both cell lines are characterized by elongated cells with the characteristic FB-like shape, as seen in electronic supplementary material, figure S3A. Subsequently, we used phalloidin staining and fluorescence microscopy, in order to characterize the actin (F-actin) cytoskeleton in each cell line. The cell cytoskeleton consists of three types of filaments (including actin

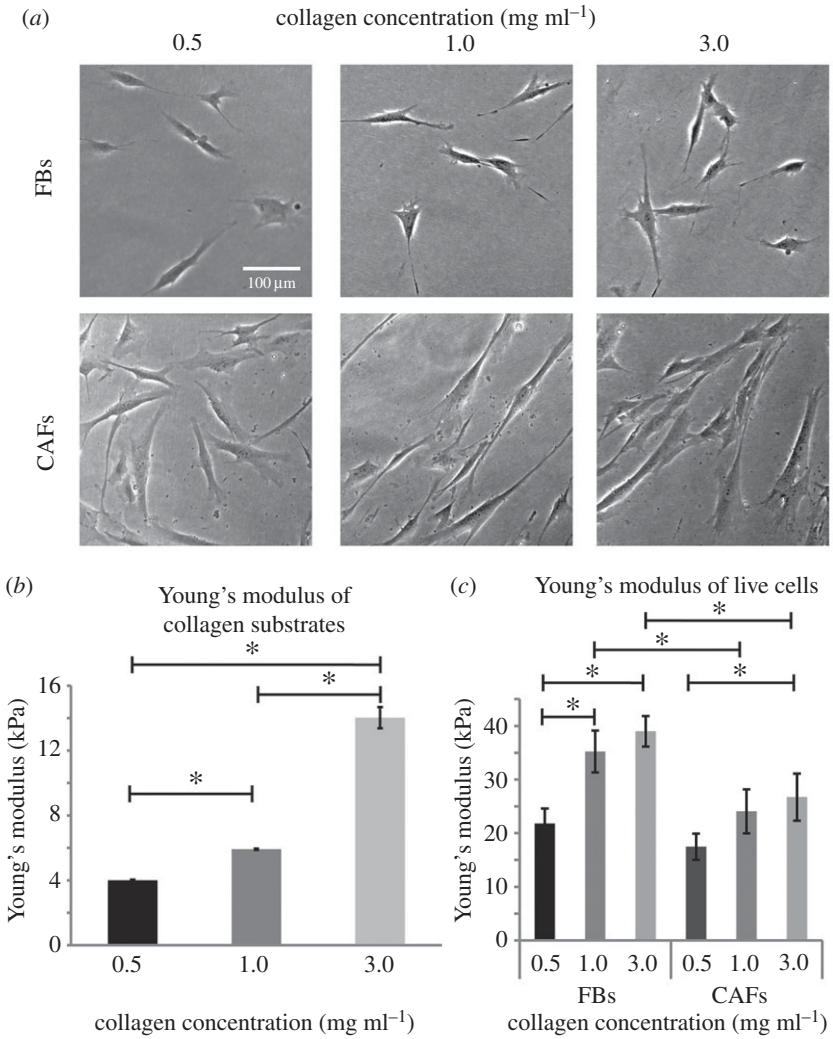

Figure 1. Effect of matrix stiffness on cell Young's modulus. (*a*) Optical microscope imaging of FBs and CAFs cultured on collagen substrates of different concentration, (*b*) relative substrate Young's modulus and (*c*) Young's modulus of live cells, measured by AFM. Asterisks indicate a statistically significant difference between compared groups ($p < 0.05$).

microfilaments, intermediate filaments and microtubules) with actin filaments being considered the most significant for modulating the mechanical properties of cells [26]. Our results demonstrated that both CAFs and FBs exhibited intense stress fibres (which refers to a qualitative measure of how strong stress fibres are stained with phalloidin), while CAFs also exhibited increased formation of lamellipodia, the sheet-like membrane protrusions involved in cell movement, suggesting that CAFs have a more migratory phenotype (electronic supplementary material, figure S3B), in agreement with previous studies [27].

As tumour stiffening is an important consequence of desmoplasia, we investigated the effect of matrix stiffness on basic cellular characteristics of pancreatic FBs and CAFs, such as cell stiffness, *α-SMA* expression (the most common FB activation marker), cell spreading and stress fibre formation and orientation. Our approach involved the preparation of collagen substrates of different concentrations which evidently exhibit different stiffness properties [21,28].

The formed substrates were used for culturing both FBs and CAFs (figure 1*a*). FBs and CAFs cultured on collagen substrates of different concentration exhibited distinct characteristics with FBs being randomly oriented in all collagen concentrations and CAFs being organized in the same orientation as substrate stiffness increases. Figure 2*b* and figure S4 (electronic supplementary material) presents the relative Young's modulus of the substrates, measured with AFM, with respect to collagen concentration, confirming the dependence of substrate elastic properties on collagen content [29]. Subsequently, as AFM is gaining ground in cell mechanics [30] and in cancer diagnostics being a novel technique for determining the mechanical properties of various cell types of different metastatic potentials [31–34], we extended our experiments to include AFM force spectroscopy in live cells cultured on different substrates. Figure 1*c* depicts the Young's modulus of FBs and CAFs as a function of collagen concentration (i.e. substrate stiffness). The Young's modulus increased with substrate stiffness for both cell lines, with changes in the modulus of FBs to be more sensitive to changes in substrate stiffness. As for the Young's modulus of CAFs, a statistically significant increase was found only for the 3.0 mg ml^{-1} collagen concentration (figure 1*c*). On the other hand, when cells were treated with Cytochalasin D, a known inhibitor of actin polymerization, their Young's moduli were not affected by the substrate stiffness and the Young's moduli of the different groups did not present statistically significant differences (electronic supplementary material, figure S5). This demonstrates that our measurements correspond to the cells stiffness and it is not an artefact of the AFM measurements.

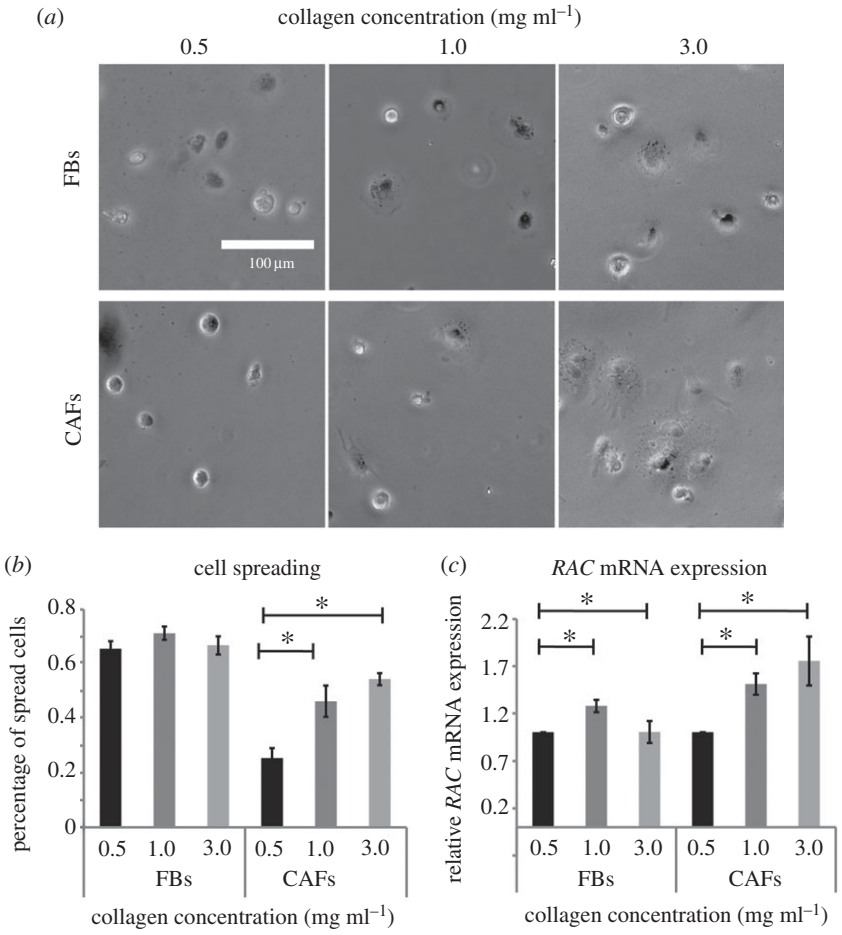

Figure 2. Substrate stiffness increases cell spreading of CAFs. (*a*) Representative optical microscope images of cells cultured on collagen substrates of different concentration. (*b*) Quantitative analysis of cell spreading using the circularity shape factor based on optical microscope images and (*c*) relative *RAC* mRNA expression assessed by real-time PCR. Asterisks indicate a statistically significant difference between compared groups ($p < 0.05$).

Notably, it has been recently demonstrated that CAFs are 'softer' compared to FBs and consequently CAFs exhibit a more aggressive phenotype [27]. Thus, our experiments confirmed that for stiffer substrates CAFs have lower values of Young's modules compared to FBs (figure 1*c*). However, this is not the case for soft substrates. Interestingly, when substrates of 0.5 mg ml^{-1} collagen were used, FBs and CAFs demonstrated similar Young's modulus values. This result highlights the fact that in desmoplastic tumours, CAFs might acquire a 'softer' and more aggressive phenotype.

3.2. Matrix stiffening increases cell spreading

Subsequently, we measured the effect of matrix stiffening on cell spreading, which is related to invasion and metastasis. Our results indicated that increased collagen concentration, and consequently increased stiffness, affects cell spreading of CAFs but not FBs. The cell spreading assay showed that cell spreading was increased in correlation to increased stiffness (figure 2*a*,*b*). We also used real-time PCR to assess *RAC* expression, as *RAC* is required for actin polymerization and is a known mediator of cell spreading [35]. Real-time PCR, which is more sensitive than optical microscopy observations, showed that stiffness affected *RAC* mRNA expression both in FBs and CAFs from 0.5 to 1.0 mg ml^{-1}, while in the case of 3.0 mg ml^{-1} *RAC* expression was increased only in CAFs (figure 2*c*).

3.3. Matrix stiffening increases α-smooth muscle actin expression in both fibroblasts and cancer-associated fibroblasts

Next, given the fact that α-SMA is the most common marker of activated FBs [36–39], we studied α-SMA expression in FBs and CAFs by means of fluorescence microscopy and real-time PCR. Figure 3*a* depicts immunofluorescence images of α-SMA protein expression and localization in FBs and CAFs and in correlation with collagen concentration and thus, substrate stiffness. Expression of α-SMA increases with substrate stiffness (electronic supplementary material, figure S6), which is in agreement with the quantitative mRNA expression of *α-SMA* analysed by real-time PCR (figure 3*b*).

3.4. Matrix stiffening improves orientation of the less oriented stress fibres of fibroblasts

To complete FBs and CAFs cytoskeletal characterization in conditions of increased substrate stiffness, we tested stress fibre orientation by F-actin staining with phaloidin. As F-actin fibre orientation has been associated with increased migration, we used the *FilamentSensor* tool software to visualize stress fibre orientation [18]. As shown in figure 4, this tool represents the direction of each fibre with a different colour. In the case of soft substrates

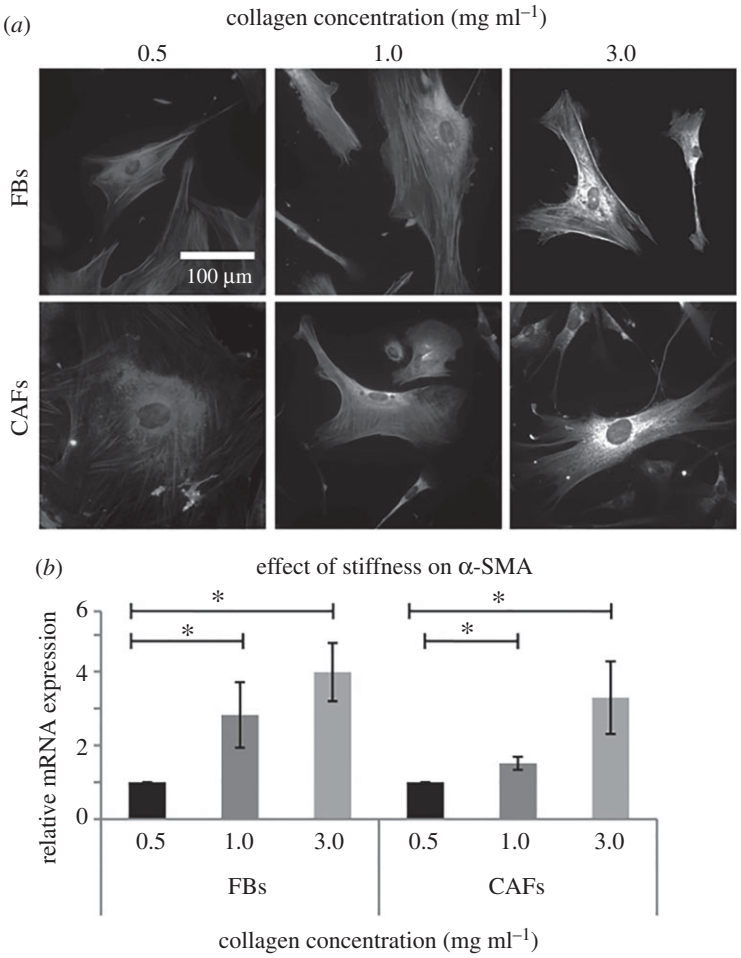

Figure 3. FBs and CAFs α-SMA expression. (*a*) Immunofluorescence images of α-SMA stained cells and (*b*) relative mRNA α-SMA expression. Asterisks indicate a statistically significant difference between compared groups ($p < 0.05$).

(0.5 mg ml^{-1}), stress fibres in FBs were randomly organized, while increasing substrate's stiffness, F-actin fibres acquired a more oriented pattern (figure 4*a*). On the other hand, CAFs independently of substrate stiffness presented well-organized stress fibres with one major orientation, parallel to the major axis of the cell (figure 4*b*). Also, the stress fibre (F-actin) orientation/alignment was assessed with the order parameter *S*. Table 1 summarizes the order parameter of FBs and CAFs on different collagen concentration substrates. In general, CAFs present a higher *S* than FBs, while the order parameter for both cell lines increases with the increase of collagen concentration (and consequently collagen stiffness)

3.5. Matrix stiffening inhibits cell spheroid invasion in three-dimensional collagen gels

Given our results from the 2D experiments, we sought to find out how the metastatic potential of FBs and CAFs was affected by ECM stiffness in a 3D set-up that better mimics real ECM and tumour setting [40] as it is evident that the tissue microenvironment regulates cancer cell motility and invasion [41]. Our experimental approach involved the formation of cell spheroids embedded in 3D gels made by purified type I collagen, with tunable stiffness.

The structure and elastic properties of gels containing 0.5, 1.0 or 3.0 mg ml^{-1} collagen were analysed using AFM, which does not destroy the gel's microstructure [29,42–45]. Figure 5*a* depicts the microstructure of the gels consisted of fibres with random orientations, similar to the ECM structure of collagen-rich tumours [46]. Additionally, collagen fibres presented the 67 nm D-band (figure 5*b*), which is a characteristic of the native forming collagen fibres and it has been proposed to be recognized by cells [47]. Furthermore, AFM microstructural analyses (figure 5*a*) revealed that changes in collagen concentration increased fibre density and gels with higher concentration consisted of fibres with larger diameters (figure 5*c*). In order to characterize the stiffness of the gels, we performed AFM analysis under liquid conditions. As expected, stiffness measured by AFM increased with increasing collagen concentration (figure 5*d*). In particular, we measured an increase in stiffness of about 1.5 and 3.7 times (compared to the 0.5 mg ml^{-1} condition), when the concentration was increased from 0.5 to 1.0 and 3.0 mg ml^{-1}, respectively.

The next step in our study was the formation of FBs and CAFs spheroids using the hanging drop method. Spheroids were embedded in the 3D collagen gels and 6 h later, images were obtained to quantify cell invasion (figure 6*a*). The analysis revealed that cell invasion was reduced as collagen concentration increased from 0.5 to 1.0 mg ml^{-1} (figure 6*b*). FBs, exhibited the same effect when gel concentration was increased from 0.5 to 3.0 mg ml^{-1} (figure 6*b*). However, CAFs invasion presented a differential response to stiffness and there was no

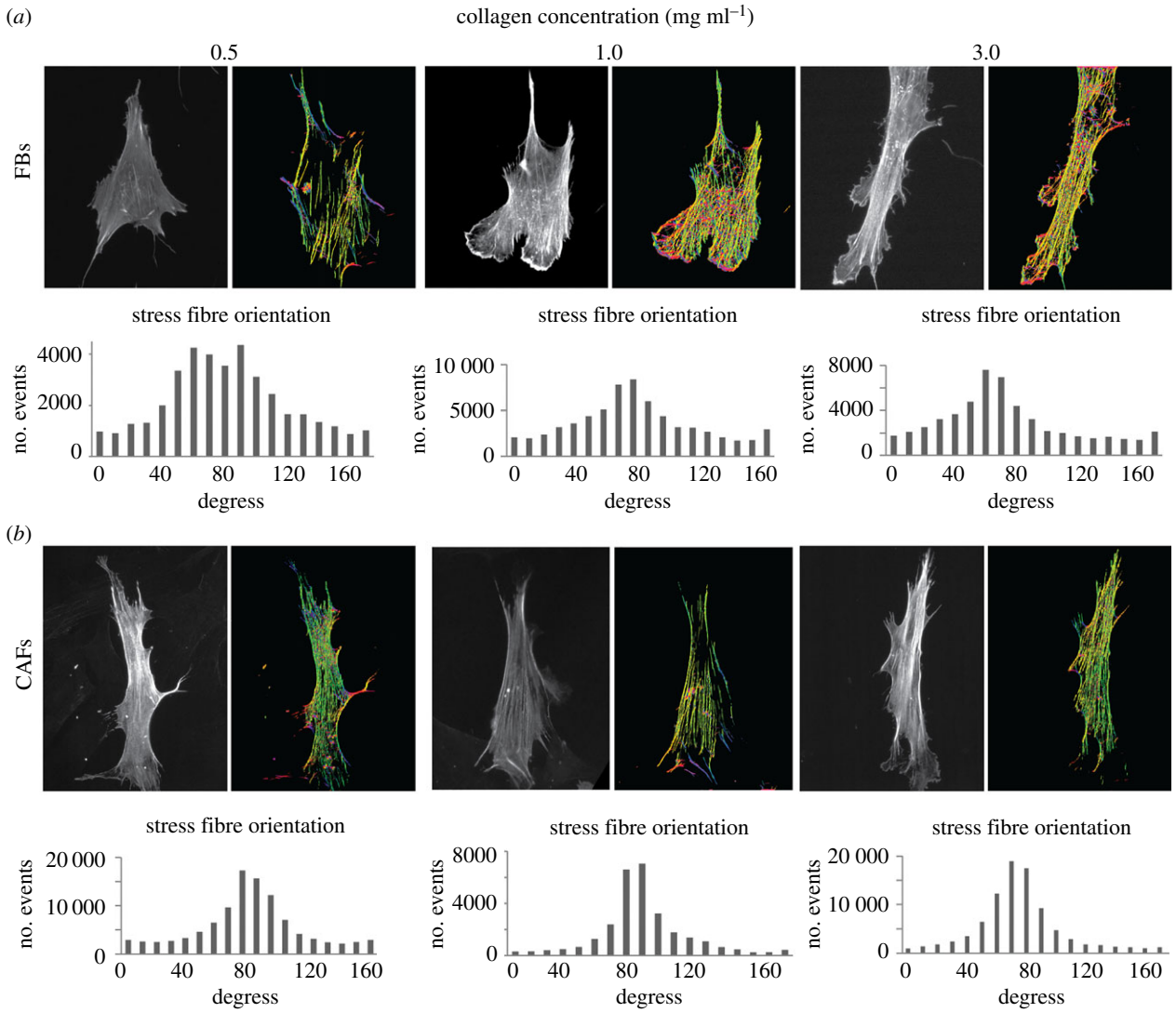

Figure 4. Effect of substrate stiffness on F-actin stress fibres of FBs and CAFs. (*a*,*b*) Phalloidin-stained cells and computationally processed images, presenting stress fibre orientation (each colour corresponds to a different fibre orientation). (Online version in colour.)

Table 1. Order parameter *S* of FBs and CAFs on substrates of different collagen concentrations.

	FBs			CAFs		
	collagen concentration (mg ml^{-1})					
	0.5	1.0	3.0	0.5	1.0	3.0
order parameter (*S*)	0.40	0.51	0.54	0.53	0.61	0.69
standard error of the mean	0.04	0.03	0.02	0.05	0.05	0.04

statistically significant alterations between the 0.5 and 3.0 mg ml^{-1} collagen concentration (figure 6*b*).

In order to investigate the molecular mechanism involved, we measured the mRNA expression of *RhoA* and *Rho-associated protein kinase-1* (*ROCK-1*), important members of the Rho GTPase family of proteins that have been previously suggested to be involved in FBs and CAFs ECM remodelling and invasion [27,48,49]. Real-time PCR analyses demonstrated that the mRNA expression of these genes in both cell lines was reduced as the collagen concentration was increased from 0.5 to 1.0 and 3.0 mg ml^{-1}, following the invasion pattern (figure 7*a*).

3.6. Transforming growth factor beta increases the invasive potential of both fibroblasts and cancer-associated fibroblasts

Given that TGF-β upregulation is an important component of desmoplasia, we investigated the effect of ECM stiffness on FBs and CAFs in the presence of TGF-β. In that regard, TGF-β treated FBs and CAFs were used for the formation of cell spheroids. The spheroids were embedded in the 3D collagen gels and images were obtained at time 0 and 6 h. In the case of FBs, we found that TGF-β significantly increased FB invasion in all collagen concentrations

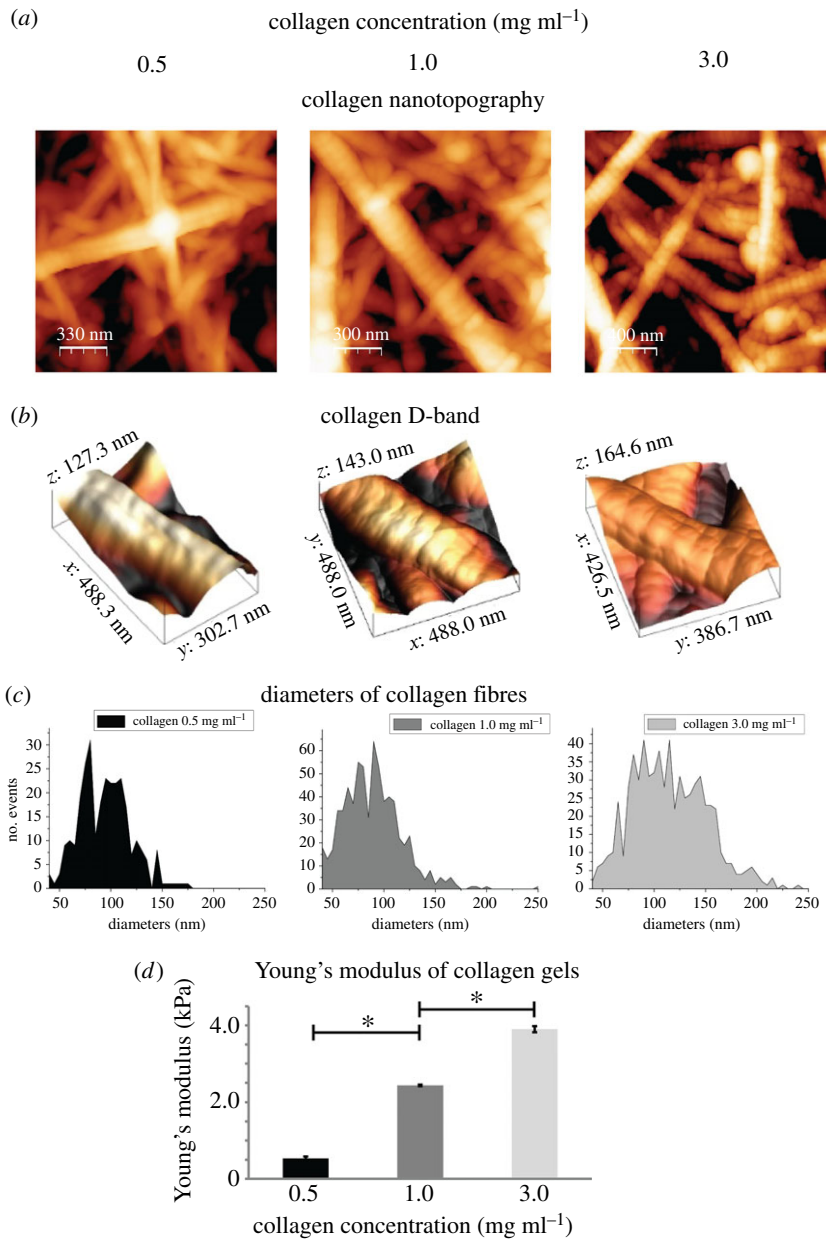

Figure 5. AFM characterization of 3D collagen matrices. (*a*,*b*) AFM topography images of collagen type I gels with different concentrations, presenting the fibre structure of the gels and the D-band (approximately 67 nm), respectively, (*c*) diameters of collagen fibres and (*d*) normalized Young's modulus of the gels relative to the Young's value of the lowest concentration. Asterisks indicate a statistically significant difference between compared groups ($p < 0.05$). (Online version in colour.)

(figure 7*c*), whereas TGF-β had negligible effects on the invasive potential of CAFs for 0.5 and 3.0 mg ml^{-1} collagen, and promoted spheroid invasion only for the 1.0 mg ml^{-1} condition (figure 7*d*). Interestingly, even though matrix stiffening reduced cell invasion (figure 6*b*), addition of TGF-β compensated for the negative effect of stiffness so that spheroid invasion remained the same for both FBs and CAFs (figure 7*c*,*d*). Real-time PCR experiments demonstrated that this effect was a consequence of the activation of the *RhoA* and *ROCK* pathway, particularly in the case of CAFs (figure 7*b*). Also, multiple comparisons between the different groups confirmed the activation effect of TGF-β on the *RhoA* and *ROCK* pathway (electronic supplementary material, figure S7).

4. Discussion

Pancreatic cancer is the leading cause of cancer-related deaths, with poor survival rates [2]. Therefore, a complete understanding of the mechanisms involved in its pathogenesis is of crucial importance. Pancreatic tumours, such as pancreatic ductal adenocarcinomas, are characterized by desmoplasia, the accumulation of increased amounts of ECM inside the tumour [2]. Although, it has been suggested that ECM stiffening modulates stromal and cancer cell properties, promotes cancer cell metastasis and hinders the effective delivery of drugs [6,7,50], the exact role of matrix stiffness in solid tumours development is not clearly defined yet [51].

As it has been demonstrated that the mechanical properties of a tumour determine cell behaviour, we investigated how collagen stiffness affects pancreatic FBs and CAFs in terms of cytoskeleton and morphodynamic characteristics re-organization as well as in terms of their invasive properties in 2D and 3D collagen models. In our *2D experiments*, we demonstrated that the Young's modulus of both FBs and CAFs increased as a function of substrate stiffness (figure 1*c*). This is in agreement with studies showing that FBs tend to tune their stiffness in order to adapt to that of

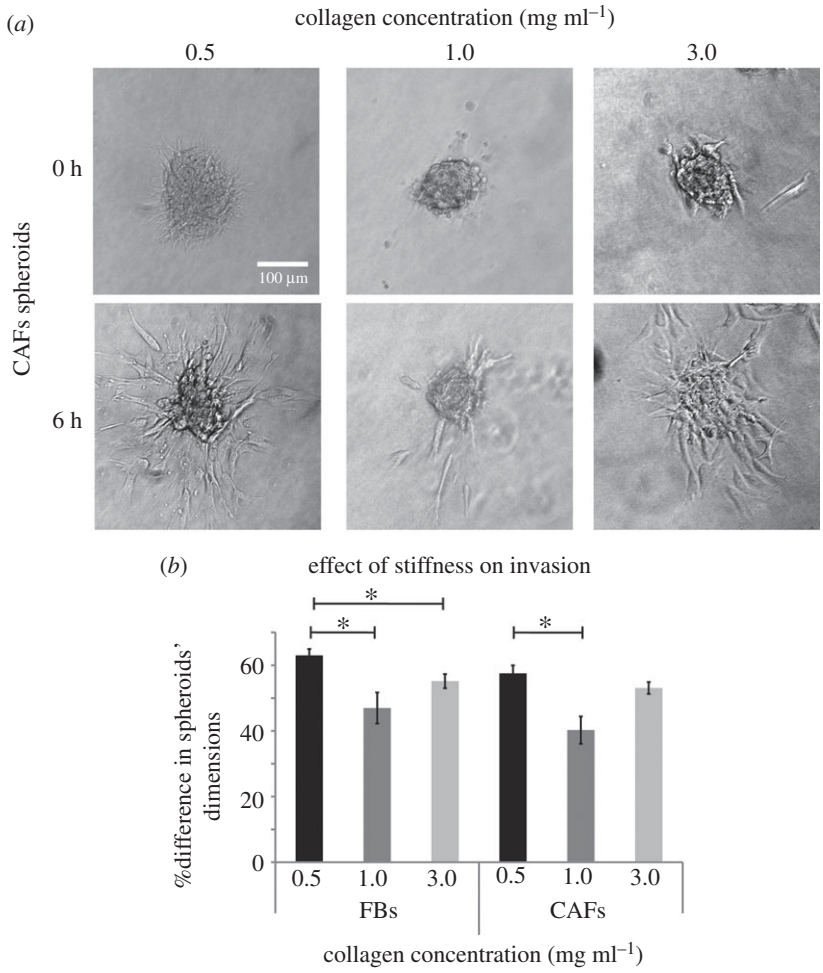

Figure 6. Effect of collagen stiffness on FBs and CAFs invasion and expression of RhoA and ROCK in the absence or presence of TGF-β. (*a*) Representative CAFs spheroids embedded in collagen gels at time 0 and at 6 h post implantation, respectively. (*b*) Percentage (%) change in FBs and CAFs spheroids' dimensions within 6 h post-implantation. Asterisks indicate a statistically significant difference between compared groups ($p < 0.05$).

their environment [52]. Indeed, when cultured on rigid substrates, CAFs proved to be softer than FBs, forming monolayers with oriented cellular patterns (figure 1). AFM studies have demonstrated that cancer cells, which are highly invasive, are also softer than normal cells [32,33], while they also remodel their cytoskeleton so as to facilitate their invasion through surrounding stiff tissues [27,53]. Similarly, we showed here that while CAFs are softer than FBs in stiff substrates and possess a more invasive phenotype reminiscent of that of cancer cells, both cell lines become stiffer in stiffer environments [54,55] when they encounter higher levels of stress. Moreover, the fact that CAFs formed oriented patterns in stiffer environments (figure 1) suggests a coordinated migratory behaviour, which ensures more effective migration than single cells [56]. Furthermore, we showed that *α-SMA* expression increased in increased substrate stiffness conditions in both cell types (figure 3 and electronic supplementary material, figure S6), confirming the hypothesis that stiffness promotes the activation of FBs into a myofibroblast-like phenotype, which is associated with a higher metastatic potential. Moreover, in accordance with previous studies showing that cells spread better on stiffer substrates [52,57], we found that CAFs, but not FBs, presented better spreading efficiency on stiffer substrates (figure 2) which was corroborated by real-time PCR analysis of *RAC* mRNA expresssion. The finding, though, that FB spreading was not affected by matrix stiffness may be explained by the fact that alterations in cell stiffness tend to affect cell spreading thus it is plausible to find that CAFs exhibited better spreading properties than FBs, as they were found to be softer. Moreover, CAFs presented oriented stress fibres regardless of substrate stiffness, while FBs had the tendency to remodel F-actin stress fibres in more oriented patterns as substrate stiffness inceased (figure 4 and table 1). This is also in accordance with previous studies showing that actin structure is not organized into stress fibres in soft substrates [52,58]. It should be noted though that such cytoskeleton remodelling is translated into changes in the mechanical properties (reduced stiffness in soft substrates) of the FBs, which can be crucial for the invasive properties of the cells [30,33,54,55,59].

Furthermore, we developed 3D collagen models to study cell invasion in a more physiologically relevant approach [40]. In our *3D experiments*, we formed tumour cell spheroids that were embedded in collagen gels of different concentration. AFM nanoscale characterization demonstrated that gels consisted of collagen fibres exhibiting the characteristic D-band periodicity and had random orientation (figure 6). As the collagen concentration increased, the gel density, stiffness and collagen fibre diameter were significantly increased, confirming previous research demonstrating that alterations in collagen concentration are translated into changes in ECM stiffness [28,40]. Concerning fibre diameters, we found a range of 50–300 nm, similar to previous studies performed

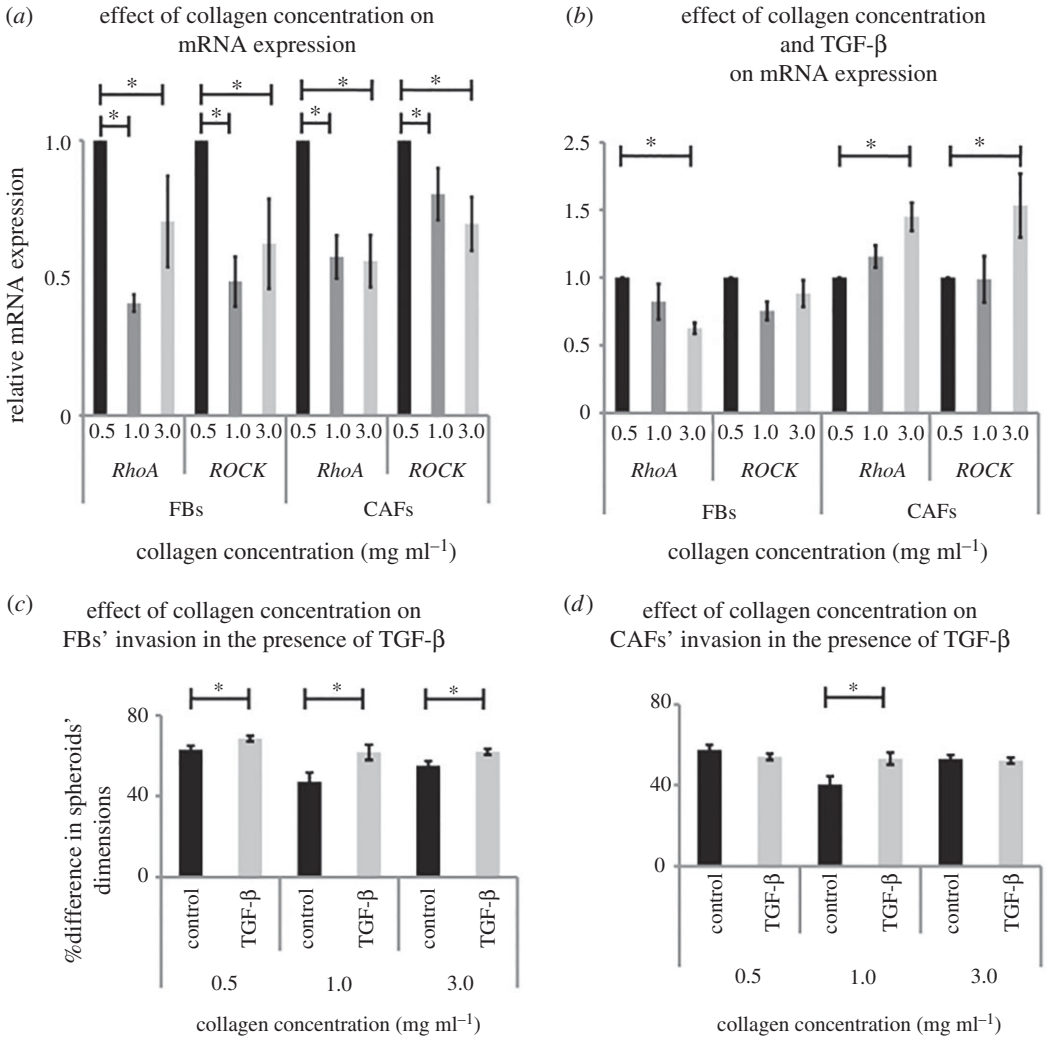

Figure 7. Effect of collagen concentration on FBs and CAFs invasion in the presence of TGF-β. (*a*) Relative *RhoA* and *ROCK* mRNA expression in cells cultured in the 3D collagen gels of different concentrations. (*b*) Relative *RhoA* and *ROCK* mRNA expression in TGF-β-treated FBs and CAFs cultured in the 3D collagen gels. (*c*,*d*) Percentage (%) change in cell spheroids' dimensions within 6 h post implantation, respectively. Asterisks indicate a statistically significant difference between compared groups ($p < 0.05$).

in high concentrated collagen gels [25] and within the range of fibre diameter of native tissues [28]. Consequently, as the Young's modulus of tissues exhibits great variability and largely depends upon the quantity and organization of collagen [47,60,61] our gels can serve as models to recapitulate tumour ECM stiffening during desmoplasia. Our results revealed that tumour spheroid invasion of FBs and CAFs was hindered when spheroids were cultured in collagen gels of higher concentration (figure 6). Thus, CAFs have most likely developed appropriate mechanisms, such as the development of oriented stress fibres and a 'softer' cytoskeleton, to be able to invade through stiff environments. Our findings were further supported by gene expression analysis showing a significant decrease in Rho-GTPases *RhoA* and *ROCK* mRNA expression in FBs and CAFs (figure 7*a*), which have been proposed to mediate cell motility, ECM remodelling by FBs [48,49] and control actin polymerization [26]. Finally, addition of TGF-β reversed the suppressive effects of stiffness on FBs and CAFs invasion (figures 7*c* and *d*), confirming the hypothesis that ECM stiffness and TGF-β have synergistic effects in desmoplasia and affect cell invasion.

Overall, our results demonstrated that collagen concentration and consequently ECM stiffening differentially modulates FBs and CAFs cytoskeleton remodelling and invasion with stress fibre orientation being significantly altered in FBs. Finally, the presence of TGF-β reverses the suppressive effect of collagen stiffness on cell invasion.

Data accessibility. This article has no additional data.

Authors' contributions. Conceptualization: A.S. and T.S., methodology: A.S. and V.G., investigation: A.S. and M.L., writing, review and editing: A.S., V.G., M.L. and T.S. All authors gave final approval for publication.

Competing interests. The authors declare no conflict of interests.

Funding. This work was supported by a Horizon 2020, Marie Skłodowska-Curie Individual Fellowship (MSCA-IF-2014-658769-MYO-DESMOPLASIA) and the European Research Council (FP7 2007–2013, ERC grant agreement no. 336839-ReEngineeringCancer).

Abbreviations

Alpha-smooth muscle actin (α-SMA)
Atomic force microscopy (AFM)
Cancer-associated fibroblasts (CAFs)
4′,6-Diamidino-2-phenylindole (DAPI)
Extracellular matrix (ECM)
Fibroblasts (FBs)
Minimal essential medium (MEM)
Paraformaldehyde (PFA)
Phosphate-buffered saline (PBS)
Ras-related C3 botulinum toxin substrate 1 (Rac)

Ras homologue family member (RhoA)
Rho-associated, coiled-coil containing protein kinase 1 (ROCK-1)
Scanning electron microscopy (SEM)
Three dimensional (3D)
Transforming growth factor-β (TGF-β)
Two dimensional (2D)

References

1. Hanahan D, Weinberg RA. 2011 Hallmarks of cancer: the next generation. *Cell* **144**, 646–674. (doi:10.1016/j.cell.2011.02.013)
2. Rath N, Olson MF. 2016 Regulation of pancreatic cancer aggressiveness by stromal stiffening. *Nat. Med.* **22**, 462. (doi:10.1038/nm.4099)
3. Voutouri C, Polydorou C, Papageorgis P, Gkretsi V, Stylianopoulos T. 2016 Hyaluronan-derived swelling of solid tumors, the contribution of collagen and cancer cells, and implications for cancer therapy. *Neoplasia* **18**, 732–741. (doi:10.1016/j.neo.2016.10.001)
4. Voutouri C, Mpekris F, Papageorgis P, Odysseos AD, Stylianopoulos T. 2014 Role of constitutive behavior and tumor–host mechanical interactions in the state of stress and growth of solid tumors. *PLoS ONE* **9**, e0104717. (doi:10.1371/journal.pone.0104717)
5. Mpekris F, Angeli S, Pirentis AP, Stylianopoulos T. 2015 Stress-mediated progression of solid tumors: effect of mechanical stress on tissue oxygenation, cancer cell proliferation, and drug delivery. *Biomech. Model. Mechanobiol.* **14**, 1391–1402. (doi:10.1007/s10237-015-0682-0)
6. Cox TR, Bird D, Baker AM, Barker HE, Ho MWY, Lang G, Erler JT. 2013 LOX-mediated collagen crosslinking is responsible for fibrosis-enhanced metastasis. *Cancer Res.* **73**, 1721–1732. (doi:10.1158/0008-5472.CAN-12-2233)
7. Jain RK, Martin JD, Stylianopoulos T. 2014 The role of mechanical forces in tumor growth and therapy. *Annu. Rev. Biomed. Eng.* **16**, 321–346. (doi:10.1146/annurev-bioeng-071813-105259)
8. Wipff PJ, Hinz B. 2009 Myofibroblasts work best under stress. *J. Bodyw. Mov. Ther.* **13**, 121–127. (doi:10.1016/j.jbmt.2008.04.031)
9. Papageorgis P, Stylianopoulos T. 2014 Role of TGFβ in regulation of the tumor microenvironment and drug delivery. *Int. J. Oncol.* **46**, 933–943. (doi:10.3892/ijo.2015.2816)
10. Wipff P-J, Rifkin DB, Meister J-J, Hinz B. 2007 Myofibroblast contraction activates latent TGF-β1 from the extracellular matrix. *J. Cell Biol.* **179**, 1311–1323. (doi:10.1083/jcb.200704042)
11. Egeblad M, Rasch MG, Weaver VM. 2010 Dynamic interplay between the collagen scaffold and tumor evolution. *Curr. Opin. Cell Biol.* **22**, 697–706. (doi:10.1016/j.ceb.2010.08.015)
12. Kalli M, Papageorgis P, Gkretsi V, Stylianopoulos T. 2018 Solid stress facilitates fibroblasts activation to promote pancreatic cancer cell migration. *Ann. Biomed. Eng.* **46**, 657–669. (doi:10.1007/s10439-018-1997-7)
13. Yamazaki D, Kurisu S, Takenawa T. 2005 Regulation of cancer cell motility through actin reorganization. *Cancer Sci.* **96**, 379–386. (doi:10.1111/j.1349-7006.2005.00062.x)
14. Cross SE, Jin Y-S, Rao J, Gimzewski JK. 2007 Nanomechanical analysis of cells from cancer patients. *Nat. Nanotechnol.* **2**, 780–783. (doi:10.1038/nnano.2007.388)
15. Papageorgis P, Polydorou C, Mpekris F, Voutouri C, Agathokleous E, Kapnissi-Christodoulou CP, Stylianopoulos T. 2017 Tranilast-induced stress alleviation in solid tumors improves the efficacy of chemo- and nanotherapeutics in a size-independent manner. *Sci. Rep.* **7**, 46140. (doi:10.1038/srep46140)
16. Polydorou C, Mpekris F, Papageorgis P, Voutouri C, Stylianopoulos T. 2017 Pirfenidone normalizes the tumor microenvironment to improve chemotherapy. *Oncotarget* **8**, 24 506–24 517. (doi:10.18632/oncotarget.15534)
17. Mpekris F, Papageorgis P, Polydorou C, Voutouri C, Kalli M, Pirentis AP, Stylianopoulos T. 2017 Sonic-hedgehog pathway inhibition normalizes desmoplastic tumor microenvironment to improve chemo- and nanotherapy. *J. Control. Release* **261**, 105–112. (doi:10.1016/j.jconrel.2017.06.022)
18. Eltzner B, Wollnik C, Gottschlich C, Huckemann S, Rehfeldt F. 2015 The filament sensor for near real-time detection of cytoskeletal fiber structures. *PLoS ONE* **10**, e0126346. (doi:10.1371/journal.pone.0126346)
19. Zemel A, Rehfeldt F, Brown AE.X., Discher DE, Safran SA. 2010 Optimal matrix rigidity for stress-fibre polarization in stem cells. *Nat. Phys.* **6**, 468. (doi:10.1038/nphys1613)
20. Tu Y, Wu S, Shi X, Chen K, Wu C. 2003 Migfilin and Mig-2 link focal adhesions to filamin and the actin cytoskeleton and function in cell shape modulation. *Cell* **113**, 37–47. (doi:10.1016/S0092-8674(03)00163-6)
21. Gkretsi V, Stylianou A, Louca M, Stylianopoulos T. 2017 Identification of Ras suppressor-1 (RSU-1) as a potential breast cancer metastasis biomarker using a three-dimensional *in vitro* approach. *Oncotarget* **8**, 27 364–27 379. (doi:10.18632/oncotarget.16062)
22. Gkretsi V, Stylianou A, Stylianopoulos T. 2017 Vasodilator-stimulated phosphoprotein (VASP) depletion from breast cancer MDA-MB-231 cells inhibits tumor spheroid invasion through downregulation of migfilin, β-catenin and urokinase-plasminogen activator (uPA). *Exp. Cell Res.* **352**, 281–292. (doi:10.1016/j.yexcr.2017.02.019)
23. Horcas I, Fernández R, Gómez-Rodríguez JM, Colchero J, Gómez-Herrero J, Baro AM. 2007 WSXM: a software for scanning probe microscopy and a tool for nanotechnology. *Rev. Sci. Instrum.* **78**, 013705. (doi:10.1063/1.2432410)
24. Hermanowicz P, Sarna M, Burda K, Gabryś, H. 2014 AtomicJ: an open source software for analysis of force curves. *Rev. Sci. Instrum.* **85**, 063703. (doi:10.1063/1.4881683)
25. Garvin KA, Vanderburgh J, Hocking DC, Dalecki D. 2013 Controlling collagen fiber microstructure in three-dimensional hydrogels using ultrasound. *J. Acoust. Soc. Am.* **134**, 1491–1502. (doi:10.1121/1.4812868)
26. Chiou YW, Lin HK, Tang MJ, Lin HH, Yeh ML. 2013 The influence of physical and physiological cues on atomic force microscopy-based cell stiffness assessment. *PLoS ONE* **8**, e77384. (doi:10.1371/journal.pone.0077384)
27. Stylianou A, Gkretsi V, Stylianopoulos T. 2018 Transforming growth factor-β modulates pancreatic cancer associated fibroblasts cell shape, stiffness and invasion. *Biochim. Biophys. Acta Gen. Subj.* **1862**, 1537–1546. (doi:10.1016/j.bbagen.2018.02.009)
28. Roeder BA, Kokini K, Sturgis JE, Robinson JP, Voytik-Harbin SL. 2002 Tensile mechanical properties of three-dimensional type I collagen extracellular matrices with varied microstructure. *J. Biomech. Eng.* **124**, 214–222. (doi:10.1115/1.1449904)
29. Kontomaris SV, Yova D, Stylianou A, Politopoulos K. 2015 The significance of the percentage differences of Young's modulus in the AFM nanoindentation procedure. *Micro Nanosyst.* **7**, 86–97. (doi:10.2174/1876402908666151111234441)
30. Trepat X, Lenormand G, Fredberg JJ. 2008 Universality in cell mechanics. *Soft Matter* **4**, 1750–1759. (doi:10.1039/b804866e)
31. Cross SE, Jin Y-S, Rao J, Gimzewski JK. 2009 Applicability of AFM in cancer detection. *Nat. Nanotechnol.* **4**, 72. (doi:10.1038/nnano.2009.036)
32. Stylianou A, Stylianopoulos T. 2016 Atomic force microscopy probing of cancer cells and tumor microenvironment components. *Bionanoscience* **6**, 33–46. (doi:10.1007/s12668-015-0187-4)
33. Lekka M. 2016 Discrimination between normal and cancerous cells using AFM. *Bionanoscience* **6**, 65–80. (doi:10.1007/s12668-016-0191-3)
34. Plodinec M *et al.* 2012 The nanomechanical signature of breast cancer. *Nat. Nanotechnol.* **7**, 757–765. (doi:10.1038/nnano.2012.167)
35. Parri M, Chiarugi P. 2010 Rac and Rho GTPases in cancer cell motility control. *Cell Commun. Signal.* **8**, 23. (doi:10.1186/1478-811x-8-23)
36. Karagiannis GS, Poutahidis T, Erdman SE, Kirsch R, Riddell RH, Diamandis EP. 2012 Cancer-associated fibroblasts drive the progression of metastasis through both paracrine and mechanical pressure on cancer tissue. *Mol. Cancer Res.* **10**, 1403–1418. (doi:10.1158/1541-7786.MCR-12-0307)
37. Calon A, Tauriello DVF, Batlle E. 2014 TGF-beta in CAF-mediated tumor growth and metastasis. *Semin.*

Cancer Biol. **25**, 15–22. (doi:10.1016/j.semcancer.2013.12.008)

38. Kalluri R. 2016 The biology and function of fibroblasts in cancer. *Nat. Rev. Cancer* **16**, 582–598. (doi:10.1038/nrc.2016.73)
39. Kalluri R, Zeisberg M. 2006 Fibroblasts in cancer. *Nat. Rev. Cancer* **6**, 392–401. (doi:10.1038/nrc1877)
40. Timraz SBH, Rezgui R, Boularaoui SM, Teo JCM. 2015 Stiffness of extracellular matrix components modulates the phenotype of human smooth muscle cells *in vitro* and allows for the control of properties of engineered tissues. *Procedia Eng.* **110**, 29–36. (doi:10.1016/j.proeng.2015.07.006)
41. Brábek J, Mierke CT, Rösel D, Veselý P, Fabry B. 2010 The role of the tissue microenvironment in the regulation of cancer cell motility and invasion. *Cell Commun. Signal.* **8**, 22. (doi:10.1186/1478-811x-8-22)
42. Stylianou A, Yova D. 2013 Surface nanoscale imaging of collagen thin films by atomic force microscopy. *Mater. Sci. Eng. C* **33**, 2947–2957. (doi:10.1016/j.msec.2013.03.029)
43. Stylianou A, Yova D, Alexandratou E. 2014 Investigation of the influence of UV irradiation on collagen thin films by AFM imaging. *Mater. Sci. Eng. C* **45**, 455–468. (doi:10.1016/j.msec.2014.09.006)
44. Stylianou A, Kontomaris SV, Yova D. 2014 Assessing collagen nanoscale thin films heterogeneity by AFM multimode imaging and nanoindetation for nanobiomedical applications. *Micro Nanosys.* **6**, 95–102. (doi:10.2174/1876402906021411271144 48#sthash.960XePnt.dpuf)
45. Stylianou A, Yova D, Politopoulos K. 2012 Atomic force microscopy quantitative and qualitative nanoscale characterization of collagen thin films. In *Proc. 5th International Conference on Emerging Technologies in Non-Destructive Testing (NDT 21012), Ioannina, Greece, 19–21 September*, pp. 415–420.
46. Ramanujan S, Pluen A, McKee TD, Brown EB, Boucher Y, Jain RK. 2002 Diffusion and convection in collagen gels: implications for transport in the tumor interstitium. *Biophys. J.* **83**, 1650–1660. (doi:10.1016/S0006-3495(02)73933-7)
47. Fratzl P. 2008 *Collagen structure and mechanics*. New York, NY: Springer.
48. Gaggioli C, Hooper S, Hidalgo-Carcedo C, Grosse R, Marshall JF, Harrington K, Sahai E. 2007 Fibroblast-led collective invasion of carcinoma cells with differing roles for RhoGTPases in leading and following cells. *Nat. Cell Biol.* **9**, 1392–1400. (doi:10.1038/ncb1658)
49. Attieh Y, Vignjevic DM. 2016 The hallmarks of CAFs in cancer invasion. *Eur. J. Cell Biol.* **95**, 493–502. (doi:10.1016/j.ejcb.2016.07.004)
50. Laklai H *et al*. 2016 Genotype tunes pancreatic ductal adenocarcinoma tissue tension to induce matricellular fibrosis and tumor progression. *Nat. Med.* **22**, 497–505. (doi:10.1038/nm.4082)
51. Kalli M, Stylianopoulos T. 2018 Defining the role of solid stress and matrix stiffness in cancer cell proliferation and metastasis. *Front. Oncol.* **8**, 55. (doi:10.3389/fonc.2018.00055)
52. Neesse A, Algül H, Tuveson DA, Gress TM. 2015 Stromal biology and therapy in pancreatic cancer: a changing paradigm. *Gut* **64**, 1476–1484. (doi:10.1136/gutjnl-2015-309304)
53. Wu TH, Chiou YW, Chiu WT, Tang MJ, Chen CH, Yeh ML. 2014 The F-actin and adherence-dependent mechanical differentiation of normal epithelial cells after TGF-β1-induced EMT (tEMT) using a microplate measurement system. *Biomed. Microdevices* **16**, 465–478. (doi:10.1007/s10544-014-9849-1)
54. Prina-Mello A, Jain N, Liu B, Kilpatrick JI, Tutty MA, Bell AP, Jarvis SP, Volkov Y, Movia D. 2018 Culturing substrates influence the morphological, mechanical and biochemical features of lung adenocarcinoma cells cultured in 2D or 3D. *Tissue Cell* **50**, 15–30. (doi:10.1016/j.tice.2017.11.003)
55. Xu W, Mezencev R, Kim B, Wang L, McDonald J, Sulchek T. 2012 Cell stiffness is a biomarker of the metastatic potential of ovarian cancer cells. *PLoS ONE* **7**, e46609. (doi:10.1371/journal.pone.0046609)
56. Mayor R, Etienne-Manneville S. 2016 The front and rear of collective cell migration. *Nat. Rev. Mol. Cell Biol.* **17**, 97–109. (doi:10.1038/nrm.2015.14)
57. El-Mohri H, Wu Y, Mohanty S, Ghosh G. 2017 Impact of matrix stiffness on fibroblast function. *Mater. Sci. Eng. C* **74**, 146–151. (doi:10.1016/j.msec.2017.02.001)
58. Flanagan LA, Ju YE, Marg B, Osterfield M, Janmey PA. 2002 Neurite branching on deformable substrates. *Neuroreport* **13**, 2411–2415. (doi:10.1097/00001756-200212200-00007)
59. Lekka M, Pogoda K, Gostek J, Klymenko O, Prauzner-Bechcicki S, Wiltowska-Zuber J, Jaczewska J, Lekki J, Stachura Z. 2012 Cancer cell recognition—mechanical phenotype. *Micron* **43**, 1259–1266. (doi:10.1016/j.micron.2012.01.019)
60. van Helvert S, Friedl P. 2016 Strain stiffening of fibrillar collagen during individual and collective cell migration identified by AFM nanoindentation. *ACS Appl. Mater. Interfaces* **8**, 21 946–21 955. (doi:10.1021/acsami.6b01755)
61. Freedman BR, Bade ND, Riggin CN, Zhang S, Haines PG, Ong KL, Janmey PA. 2015 The (dys)functional extracellular matrix. *Biochim. Biophys. Acta Mol. Cell Res.* **1853**, 3153–3164. (doi:10.1016/j.bbamcr.2015.04.015)